Inherent issues regarding the use of *in situ* x-ray diffraction measurements to determine temperature in shock-compressed metals

Surinder M. Sharma[1] and Yogendra M. Gupta [1,2]

[1]*Institute for Shock Physics, Washington State University, Pullman, Washington 99164, USA*
[2]*Department of Physics and Astronomy, Washington State University, Pullman, Washington 99164, USA*

Temperature determination in shock-compressed solids constitutes an important and long-standing scientific need. Since the reduction of Bragg diffracted peaks due to temperature increase, using the Debye-Waller factor, is well established, we examined the use of this approach to determine temperatures in shock-compressed gold and platinum by representing the shocked state as a superposition of density and temperature changes. Comparison of the calculated and measured diffraction peaks did not show good agreement, because x-ray diffraction (XRD) profiles in the shock-compressed state are not governed solely by density and temperature changes. XRD results are also influenced measurably by shock wave induced microstructural changes. Our results demonstrate that contributions from microstructural changes need to be incorporated and modeled in the theoretical analysis to use XRD measurements for reliable temperature determination in shock-compressed solids.

I. INTRODUCTION

Shock wave experiments are uniquely suited to examine the real-time response of materials to high pressures and temperatures. Use of the Rankine-Hugoniot jump conditions results in a determination of the longitudinal stress, density, and internal energy—but not temperature—in the shock-compressed state [1]. Experimental determination of temperature in shock-compressed materials has long been recognized as an important and fundamental need for the development of a complete equation of state.

Over the past several decades, optical pyrometry has been the most common approach to determine temperature rise in shocked solids [2–9]. In this approach, measurements of emitted radiation are obtained at several discrete wavelengths and the measured spectra are interpreted as gray-body radiation to estimate temperatures. Although various limitations regarding optical pyrometry—measurements limited to optical penetration depth, need for improved understanding of wavelength-dependent emissivity, nonthermal emissions from extraneous sources, and heterogeneous inelastic deformation—have been discussed in the cited publications, ongoing improvements in optical pyrometry constitute an active area of research due to the importance of temperature determination in shocked solids. Recent developments regarding pyrometry measurements can be seen in Refs. [7–9].

Among optical methods, time-resolved Raman spectroscopy offers an alternate approach to temperature measurements under shock compression [10–12]. By measuring the ratios of the intensities of anti-Stokes and Stokes peaks in the same experiment, shock temperatures can be obtained up to several thousand kelvin in transparent samples. Although Raman spectroscopy likely constitutes an optimal approach, when usable, the transparency requirement for samples and

the difficulty in using it at higher temperatures—due to thermal emission [13]—precludes its general use except in fairly limited situations.

Neutron resonance broadening, assuming a hydrodynamic response and a classical assemblage of noninteracting particles, has also been proposed for temperature determination of shocked solids [14]. However, the difficulties in adapting it to common experimental configurations have likely limited its usage.

With recent experimental developments in obtaining reliable *in situ* x-ray diffraction (XRD) data in shock-compressed solids [15–17], XRD measurements represent a potentially attractive approach [18] to determine temperatures in shocked solids. We note that the effect of temperature on XRD profiles at ambient pressure is reasonably well understood [19–22]. If XRD measurements can be used reliably to determine temperatures in shocked solids, then comparisons between temperatures obtained using two very different approaches—XRD and optical pyrometry—provide a path forward for establishing confidence in measured shock temperatures.

To evaluate the use of XRD results for determining shock temperatures—the thrust of the present study—we assumed the shocked state to be a superposition of only density and temperature increases. Using this assumption, common in high-pressure shock wave studies, we have compared the calculated and measured XRD profiles in two fcc metals shock compressed to above 100 GPa. We note that our assumption regarding the shocked state is also an underlying assumption in the shock temperature measurement approaches referenced above.

Shock compression of solids beyond the Hugoniot elastic limit invariably results in microstructural changes due to plastic deformation—in addition to density and temperature changes. Hence, it is important to ascertain whether the

deduced shock temperatures are insensitive to shock-induced microstructure changes.

The remainder of the paper is organized as follows: theoretical background relevant to the calculations of the XRD profiles is presented in Sec. II. The calculated and experimental XRD profiles for shock-compressed gold and platinum are compared in Sec. III. Discussions and conclusions related to the present work are presented in Sec. IV. Supplementary details relevant to Sec. III are presented in the Appendix.

II. THEORETICAL BACKGROUND

The effect of temperature increase on the x-ray diffraction results in a crystalline solid is represented by the Debye-Waller factor, also called the temperature factor [22,23]. This factor represents the reduction in the intensities of the coherent elastically diffracted x rays, the Bragg diffraction peaks. The intensity reduction arises due to the temperature-induced increase of the atomic vibrations amplitudes. The underlying theoretical background for determining the intensity reduction is briefly discussed below.

A. Debye-Waller factor

The x-ray intensities for the Bragg diffraction peaks at a finite temperature can be written as [22,23]

$$I_T = I_0 \exp(-2M). \tag{1}$$

Here I_0 is the diffracted intensity in the absence of lattice vibrations and the Debye-Waller factor, denoted by $\exp(-2M)$, represents the effect of lattice vibrations on the intensities of the Bragg peaks. It is known that $2M = G_{hkl}^2 \langle u^2 \rangle$, where G_{hkl} represents the reciprocal lattice vector of the crystal corresponding to the hkl Bragg peak and $\langle u^2 \rangle$ represents the average mean-squared amplitude of vibrations of atoms comprising the solid [22,23]. For an anisotropic crystal, $\langle u^2 \rangle$ is a 3×3 matrix and could be represented as an ellipsoid for each atom in the unit cell [22]. For a pure metallic solid, within the harmonic approximation, the relation between $\langle u^2 \rangle$ and the vibrational modes of the solid is given as [22]

$$\langle u^2 \rangle = \frac{1}{3mN} \sum_{jq} \frac{E_j(q)}{\omega_j^2(q)}. \tag{2}$$

Here N is the number of atoms in the crystal, m the mass of the atom, $\omega_j(\mathbf{q})$ is the phonon frequency in the jth branch and at a wave vector $\mathbf{q}$, $E_j(\mathbf{q})$ is the energy of the phonon mode $[= (n + 1/2)\hbar\omega_j(q)$, n being the Bose-Einstein distribution function representing the occupancy of the vibrational states], and the sum is over all the branches and $\mathbf{q}$ vectors in the Brillouin zone. The form of $E_j(\mathbf{q})$ implies that at low temperatures the quantum effects are important but at high temperatures, when the occupancy of the vibrational states is much higher, their relevance decreases correspondingly.

Equations (1) and (2) imply that for a metallic solid at ambient pressure, a reliable calculation of the Debye-Waller factor requires a knowledge of the vibrational spectrum of the metal [22]. Specifically, calculations of the density of vibrational states should incorporate the anharmonic effects, since their noninclusion may cause significant errors [22].

B. Debye approximation

Although accurate information about the lattice vibrational states is required for detailed calculations of the Debye-Waller factor, a reasonable determination can be made by employing the Debye approximation for monatomic solids [19,20]. The Debye approximation treats the lattice vibrations as elastic modes in which the phonon energy is linearly proportional to the wave vector: $\hbar\omega(q) \sim Aq$ for $q < q_D$. Here A is a constant and q_D is the radius of the Debye sphere—defined by $\frac{4\pi}{3}q_D^3$=Brillouin-zone volume. The Debye temperature T_D is defined by the highest vibrational state, *viz.*,

$$k_\beta T_D = \hbar\omega_D = Aq_D.$$

Within the Debye approximation, $\langle u^2 \rangle$ can be written as [22]

$$\langle u^2 \rangle = \frac{3\hbar^2}{mk_\beta T_D}\left(\frac{\Phi(x)}{x} + \frac{1}{4}\right), \tag{3}$$

where $x = T_D/T$ and $\Phi(x) = \frac{1}{x}\int_0^x \frac{y\,dy}{(e^y - 1)}$.

In terms of temperature, Eq. (3) can be written as

$$\langle u^2 \rangle = \frac{3\hbar^2 T}{mk_\beta T_D^2}\left(\Phi\left(\frac{T_D}{T}\right) + \frac{1}{4}\frac{T_D}{T}\right). \tag{4}$$

Thus, the Debye approximation for a monatomic solid gives $2M$ as

$$2M = (G_{hkl})^2 \langle u^2 \rangle = \frac{3\hbar^2 G_{hkl}^2 T}{mk_\beta T_D^2}\left(\Phi\left(\frac{T_D}{T}\right) + \frac{1}{4}\frac{T_D}{T}\right). \tag{5}$$

Using $G_{hkl} = \frac{4\pi \sin\theta}{\lambda}$ (where λ represents the wavelength of x rays and θ the angle of incidence with respect to the crystal lattice planes corresponding to the Bragg diffraction peak), we get

$$2M = \frac{48\pi^2\hbar^2 T}{mk_\beta T_D^2}\left(\Phi\left(\frac{T_D}{T}\right) + \frac{1}{4}\frac{T_D}{T}\right)\left(\frac{\sin\theta}{\lambda}\right)^2. \tag{6}$$

The second term in the parentheses in Eqs. (4)–(6) represents quantum effects, which would be important for evaluating the Debye-Waller factor for T less than or close to T_D.

C. Combined temperature and pressure effects

Equations (1)–(6) show that as the average squared amplitude of atomic vibrations increases with temperature, the intensity of the Bragg diffracted peaks decreases. Several measurements on simple solids at ambient pressure have shown that, if the vibrational density of phonon states is accurately known, the calculated Debye-Waller factors match well with the experimental results [19–22]. These calculations also require inclusion of anharmonic effects, which change G_{hkl}^2 as well as the vibrational spectrum as a function of temperature [21,22].

For monatomic metals at ambient pressure, Eqs. (5) and (6), using the Debye approximation, have provided reasonable estimates of the Debye-Waller factor at intermediate temperatures, close to the Debye temperature [19,20]. At higher temperatures, the Debye temperature is temperature dependent, which arises partly from noninclusion of the thermal expansion caused by anharmonic interactions

[19–22]. However, a reliable empirical approach to obtain the temperature-dependent variation in T_D is not known.

In general, the x-ray scattering form factor [part of I_0 in Eq. (1)] decreases with increasing magnitude of the q vector. Therefore, the Bragg diffracted intensities should decrease under isothermal compression. Moreover, under isothermal compression, $|G_{hkl}|$ increases and so does T_D [24,25]. Equation (5) implies that it is the relative change in the ratio $|G_{hkl}|/T_D$ which determines the rate at which the intensities of the Bragg peaks decrease with temperature.

To obtain quantitative estimates of the changes in the intensities of the Bragg peaks within the Debye approximation, under isothermal or shock compression (superposition of pressure and temperature), we require knowing the Debye temperature as a function of volume compression. Static pressure experiments show that T_D increases with volume compression [24,25]. Under shock compression, volume-dependent changes in T_D can be estimated using the Mie-Grüneisen equation of state [24,25],

$$\Gamma(V) = \Gamma_0 \left(\frac{V}{V_0} \right)^q. \tag{7}$$

$\Gamma(V)$ is related to the Debye temperature through

$$\Gamma(V) = -\frac{\partial \ln T_D}{\partial \ln V}. \tag{8}$$

This gives

$$T_D = T_{D0} \exp[(\Gamma_0 - \Gamma)/q]. \tag{9}$$

To summarize, we note that a rigorous determination of the Debye-Waller factor requires an accurate knowledge of the density and temperature-dependent vibrational spectrum of the solid. Then, Eq. (2) can be used to obtain the average mean-squared amplitude of the vibrations. Because G_{hkl} can be determined from the $P-V$ data, the reduction in the intensities of the Bragg peaks can be calculated subsequently.

The rigorous approach indicated above is beyond the scope of the present work—intended to examine the potential of using Bragg diffraction results as a temperature probe of the shock-compressed state. Our simplified approach utilizes the following assumptions: the Debye approximation for the vibrational modes; compression variations in T_D can be evaluated using Eqs. (7)–(9); and the shocked state (at high pressures) can be viewed as a superposition of pressure and temperature. These assumptions are reasonable for evaluating the use of *in situ* x-ray diffraction for temperature determination in shock-compressed solids.

III. COMPARISON WITH EXPERIMENTAL RESULTS

To evaluate the use of *in situ*, x-ray diffraction measurements for determining temperatures under shock compression, the calculated Bragg peaks are compared with recently published experimental measurements on shock-compressed gold and platinum. These two soft monoatomic cubic metals—which retain their ambient fcc structure to significant compression [26,27]—are near ideal for such comparisons because of the considerable body of available experimental and theoretical work relevant to their response under adiabatic (shock) and isothermal (static) compression.
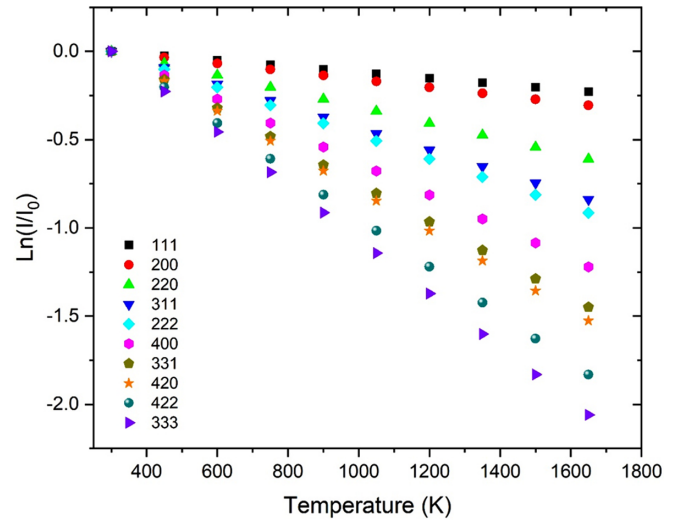

FIG. 1. Ambient pressure calculations showing the effect of increasing temperature on the integrated intensities of the ten lowest 2θ peaks of gold, using the Debye approximation for lattice vibrations.

A. Gold

Before comparing the calculated diffraction profiles with the measured profiles, we present systematics regarding the effect of temperature on Bragg peaks using gold as an example. In calculating the temperature effect, we carried out simulations of the diffraction profiles using the experimental layout commonly used in laser shock experiments conducted at the Dynamic Compression Sector, Advanced Photon Source [17]. In a typical experiment conducted on gold [28], the x rays were incident at an angle of $\sim38°$ on ~8-μm-thick gold foils. (See Fig. 6 in the Appendix for the x-ray photon flux used in the experiments and in the present calculations.) The calculations incorporated the absorption of x rays in the sample and a Lorentzian with a half width at half maximum of 250 μm to generate diffraction profiles in agreement with the measurements at ambient conditions. Further details regarding the gold experiments can be seen in Ref. [28].

The calculated first ten diffraction peaks of gold at ambient conditions are shown (see Fig. 7). The calculated results show that several peaks have significant overlap and the intensities of the higher 2θ peaks are significantly smaller than the lower 2θ peaks.

Figure 1 shows the temperature-caused reductions in the integrated intensities under each of the first ten diffraction peaks of gold at ambient pressure. The calculated results show that the intensity reductions are larger for the higher 2θ peaks than for the lower 2θ peaks. However (see Fig. 7), the higher 2θ peaks have significantly lower initial intensities and are not measurable in current shock experiments. We note that the calculated results shown in Fig. 1 and in subsequent figures are based on the assumptions listed at the end of Sec. II.

To calculate changes in the Bragg intensities of gold under isothermal compression and shock compression (superposed temperature and pressure increase), we used the known P-V results [28], $T_{D0} = 176$ K [25] and q and Γ_0 in Eq. (9), as 1.0 and 3.05, respectively [29]. The temperature increase in
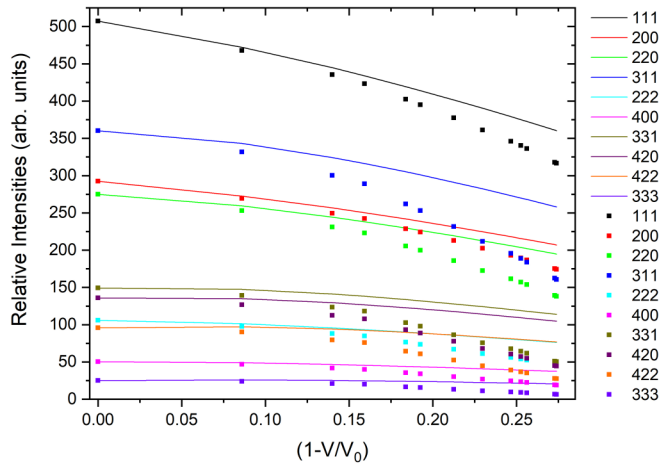
FIG. 2. Calculated variations of the integrated intensities for the ten lowest 2θ Bragg peaks of gold under isothermal compression at ambient (300 K) temperature (lines) and under shock compression (symbols), using the Debye approximation for lattice vibrations. The variations for different *hkl* peaks under isothermal and shock compression are represented by the same color.
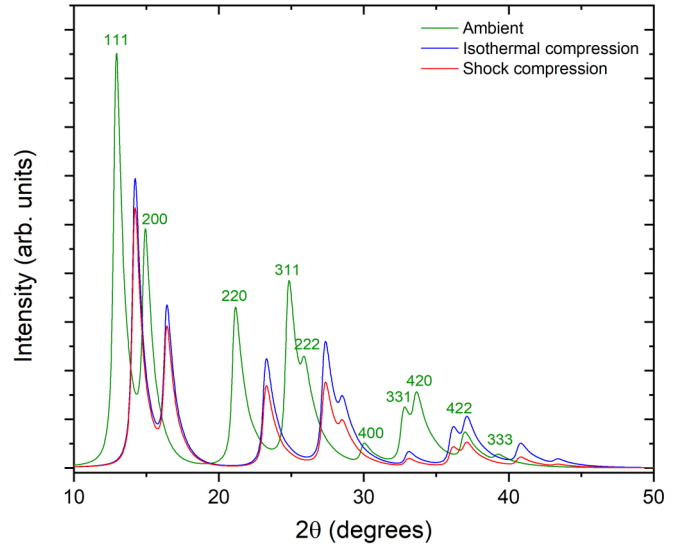

FIG. 3. Comparison of the calculated diffraction profiles of gold at ambient (green), isothermal compression (blue), and shock compression (red) using the Debye approximation for the lattice vibrations. Isothermal and shock compression results correspond to $V/V_0 = 0.752$ (shock stress of 120.3 GPa). Even isothermal compression shows significant reduction in the intensities of all the Bragg peaks with respect to the ambient. Temperature (2678 K) associated with shock compression causes a further reduction of the diffracted intensities. Ambient diffraction peaks are marked with the *hkl* indices.

shock-compressed gold was estimated using the theoretical results of Greeff and Graf [30]. For gold, our calculations showed that $|G_{hkl}|/T_D$ [Eq. (5)] decreases with compression though individually $|G_{hkl}|$ and T_D increase.

Figure 2 shows the reduction in the calculated integrated intensities of the first ten diffraction peaks as a function of volume strain $(1-V/V_0)$ under isothermal compression (300 K)—represented by the lines. Treating shock compression as a superposition of pressure and temperature increase, the calculated results under shock compression—represented by the symbols—are also shown in Fig. 2. Overall, these calculations clearly show that the intensities of the Bragg peaks are measurably reduced under shock compression beyond ∼15% compression—the compression threshold that marks the onset of significant temperature increase under shock compression [31]. Thus, to deduce temperature increase from the measured Bragg peaks, under superposed pressure and temperature increase, the reduction resulting from only the compression part needs to be carefully accounted for. In the absence of a structural transformation, compression can be unambiguously determined through the shift of the Bragg peaks. Thus, forward simulations incorporating compression and temperature effects can then be compared with the XRD measurements to deduce temperatures in the shocked state.

Before attempting to determine the temperature of a shocked sample from the experimental data, we compare the expected intensity changes of the idealized Bragg peaks under isothermal and shock compression of gold in Fig. 3. The calculated peaks (corresponding to the x-ray photon flux seen in Fig. 6) were obtained for a shock pressure of 120.3 GPa, which results in $1-V/V_0 = 0.248$. We chose this pressure because gold remains in the fcc phase at 120.3 GPa and because of available Hugoniot and XRD data [26]. Under shock compression, this pressure corresponds to a calculated temperature of 2678 K in gold [30].

Figure 3 shows that, as expected, isothermal compression results in a significant intensity reduction of all the Bragg peaks and a further reduction occurs due to the higher temperature (2678 K) under shock compression. Additionally, we make the following observations: the Bragg peaks overlap and the overlaps will change with compression; as noted earlier, the peaks at higher 2θ angles show larger reductions but the significantly lower initial intensities of these peaks make their measurements difficult.

With the current experimental capabilities, only five diffraction peaks (111, 200, 220, 311, 222) can be measured in shock-compressed Au and Pt [26–28]. In the remainder of this paper, we will consider only these five peaks and calculations of the full diffraction profiles (instead of integrated intensities shown in Figs. 1 and 2) will be compared with the experimentally measured diffraction profiles.

To compare the calculated line profile (present work) and the measured profile in the 120.3-GPa experiment on gold [28], we note that several features integral to the experimental measurements (x-ray photon flux, sample texture, shock propagation in the sample, detector location, etc.) need to be carefully accounted for in obtaining the x-ray line profiles from the experiments. Detailed procedures to account for each of these features can be seen in Ref. [28]. Because the ambient XRD data showed significant texture in the gold foils, the relative weight of each diffraction peak was adjusted to provide a good fit to the measured ambient data (see Fig. 8). Since our interest is in evaluating the role of density compression and temperature increase on the calculated diffraction profiles, the relative weights of the peaks (to account for texture at ambient
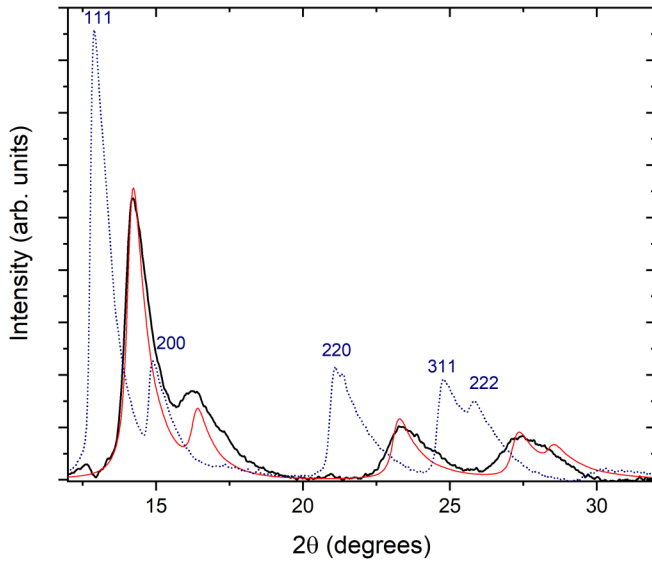
FIG. 4. Comparison of the experimental x-ray diffraction data with the calculated results for gold. Solid black line: experimental data for shock-compressed gold (120.3 GPa). Solid red line is the calculated diffraction pattern at $V/V_0 = 0.752$ (120.3 GPa) and temperature of 2678 K under shock compression. For comparison, the experimental x-ray diffraction line profile for gold at ambient conditions is also shown as the blue dotted curve.
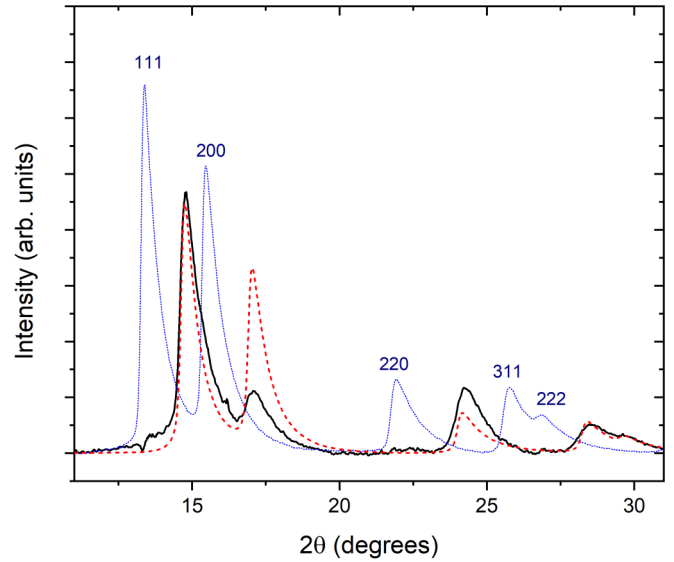

FIG. 5. Comparison of the experimental x-ray diffraction data with the calculated results for platinum. Solid black line: experimental data for shock-compressed Pt (200.9 GPa). Dashed red line is the calculated diffraction pattern at $V/V_0 = 0.7466$ (200.9 GPa) and temperature of 3190 K under shock compression. For comparison, the experimental x-ray diffraction line profile for Pt at ambient conditions is also shown as the blue dotted curve.

conditions) under shock compression was kept the same as at the ambient conditions.

Figure 4 shows a comparison of three diffraction profiles: experimental data at ambient conditions; calculated results accounting for density compression and temperature increase; and experimental data under shock compression. Although the measurement under shock compression shows reduction of the diffracted intensities for all five Bragg peaks when compared to the ambient measurement, a detailed comparison of the calculated peaks and the measured peaks does not show the good agreement required to determine the temperature in the shocked state. This difficulty is accentuated by the fact that even increasing or decreasing the calculated temperature by 1000 K does not result in noticeable improvements in the comparison with the measured peaks (see Fig. 9). Essentially, the comparisons between the calculated peaks and the measured peaks (Fig. 4 and see Fig. 9) show that the diffraction peaks in shock-compressed gold are not governed solely by density compression and temperature increase. Without accounting for the role of the other factors contributing to the diffraction data, a good determination of temperature is not possible from the measured diffraction peaks in shock-compressed gold.

The most notable difference between the calculated and the measured results is that the measured diffraction peaks are significantly broader than the calculated peaks. Also, the intensity of the measured (200) peak is larger than the calculated (200) peak. The large generation of stacking faults has been established previously in shock-compressed gold [28], and the same can account for the small shifts observed in the position of the (200) and (222) peaks. To rule out the possibility that the observed disagreements for gold are due

to the abundance of stacking faults in shock-compressed gold, the approach used for gold can be applied to platinum which does not have significant abundance of stacking faults in the shock-compressed state [27].

B. Platinum

X-ray diffraction results on shock-compressed Pt have been obtained [27] using an experimental approach similar to the experiments on gold [28]. The x-ray photon flux used to obtain diffraction data in shock-compressed Pt is also shown (see Fig. 6). Because Pt retains the fcc structure to significantly higher stresses [27], we chose to examine the Pt response for the experiment at 200.9 GPa.

Similar to gold, the Debye temperature of Pt increases with compression and its variation is calculated using Eq. (9). For Pt, $T_{D0} = 230$ K, $\Gamma_0 = 2.7$, and $q = 1.1$ [32]. For a shock stress of 200.9 GPa, $V/V_0 = 0.7466$ [27] and the estimated temperature is 3190 K [33].

The ambient diffraction pattern of Pt, similar to Au, displayed texture. The relative weights of the five diffraction peaks were optimized through independent scaling to account for the texture. The calculated profile matches very well the measured profile at ambient conditions (see Fig. 10). Similar to the Au calculations, texture changes were not considered in calculating the Pt diffraction under shock compression.

Figure 5 shows a comparison of the calculated and measured diffraction peaks for shock-compressed Pt—along with the measured diffraction peaks at ambient conditions. Except for the superposed peaks (311) and (222), the other peaks show considerable differences. Similar to the gold results, the measured peaks in Pt are broader. Furthermore, the relative

intensities of the peaks differ significantly. For the (200) peak, the measured peak is much smaller than the calculated peak. In contrast, the measured (220) peak is larger than the calculated (220) peak. Because of the large differences between the measured and calculated results, the diffraction peaks in shock-compressed Pt are also not solely governed by density compression and temperature increase. Without properly accounting for other factors contributing to the diffraction results, temperatures cannot be determined from the diffraction peaks in shock-compressed Pt.

IV. DISCUSSION AND CONCLUDING REMARKS

The use of *in situ* x-ray diffraction measurements to reliably determine temperatures under shock compression requires that good agreement should be achieved between the measured peaks and the corresponding calculated peaks. As seen in Sec. III, good agreement was not achieved for either Au or Pt. Two key differences—line broadening and changes in the relative weights of the diffraction peaks—cannot be attributed to the use of the Debye approximation, since the Debye-Waller factor formulation does not contribute to either of these differences. Even if details of the lattice vibrations are incorporated in the calculations, including anharmonic effects, that will result in a different value of the averaged mean-squared amplitude of the lattice vibrations—resulting in a different temperature. A change of ± 1000 K does not improve the agreement (see Fig. 9). Thus, incorporation of the detailed vibration spectrum cannot account for the differences presented in Figs. 4 and 5.

The lack of good agreement between the calculated and measured peaks for both metals shows that shock wave induced changes in the diffraction profiles are not determined solely by temperature and density increase—and other shock-induced changes need to be considered and accounted for in the diffraction calculations. The same are briefly discussed next.

In particular, changes in the relative weights of the diffraction peaks with respect to the ambient values imply texture changes under shock compression. As noted in previous sections, temperature determination using XRD is based on a comparison of the intensities. Therefore, without reliably modeling shock wave induced texture changes in the partially textured metal samples, XRD measurements cannot be used for temperature determination under shock compression. Whether this limitation as well as effects of other microstructural changes can be circumvented by performing measurements on samples specially prepared to ensure absence of preferred crystallite orientations in the initial state will require further investigations.

The second difference—the increased broadening observed in the measured Bragg peaks—is likely a fundamental attribute of shock compression of solids. Beyond the Hugoniot elastic limit, shock compression causes inelastic deformation resulting in significant microstructural changes; the generation of dislocations [34], stacking faults [28,35], twinning [36], and other material-specific defects would cause a reduction in the dimensions of the coherently diffracting domains leading to an inherent broadening of the peaks. A comprehensive and predictive understanding of this feature is required to establish the use of XRD for reliable temperature determination in shock-compressed samples.

Based on the findings presented for Au and Pt in this work, we conclude that the results of x-ray diffraction measurements in shock-compressed metals depend on shock wave induced density, temperature, and microstructural changes. Hence, quantitative theoretical modeling of the microstructural changes and their effect on XRD profiles is required—in addition to the developments presented here—to use XRD results for temperature determination in shocked solids. Although a challenging undertaking, the potential use of molecular-dynamics simulations for modeling microstructural changes would be desirable and worth exploring, given the importance of temperature determination under shock compression.

Although one can argue that findings based on Au and Pt cannot be generalized to all materials (even all metals), we chose Au and Pt because they appeared to be well suited—for reasons noted earlier—for using XRD measurements to determine temperature under shock compression. Finally, we note that the approach and results presented here provide a path forward to evaluate the use of XRD measurements for shock temperature determination in other candidate materials, particularly for materials/conditions where the XRD results may be insensitive to microstructural changes.

APPENDIX

Here we provide Figs. 6–10 that constitute supplementary details relevant to the calculations and analysis presented in Sec. III.
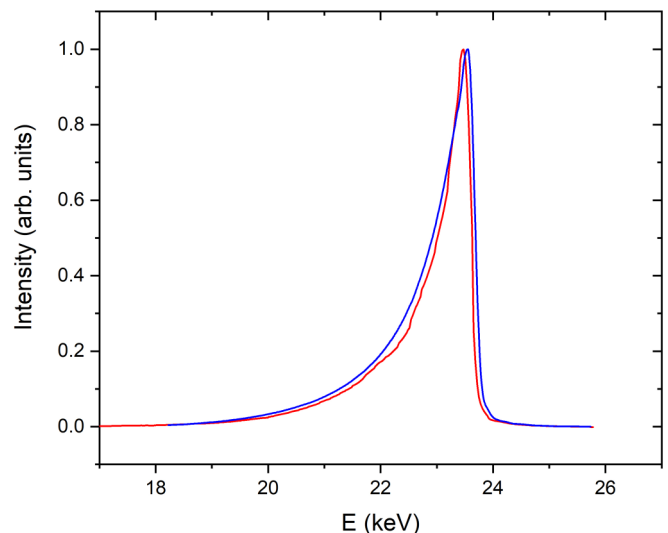

FIG. 6. Representative measured x-ray flux spectra used in x-ray diffraction experiments on laser shock-compressed gold (red) and platinum (blue).
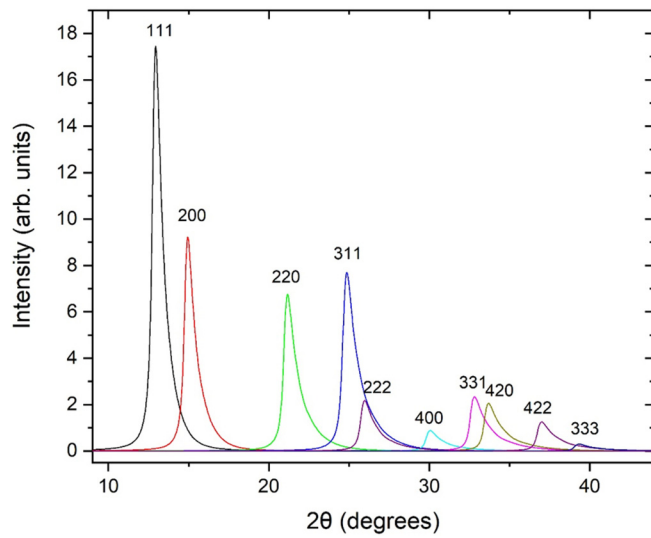
FIG. 7. Calculated XRD profile showing the first ten peaks of gold at ambient conditions.
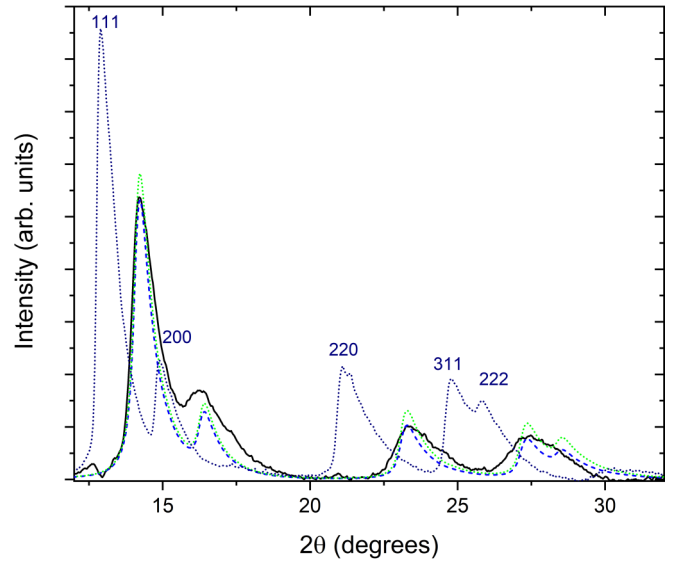

FIG. 9. Comparison of measured x-ray diffraction peaks with the calculated peaks for gold. Solid black line: experimental data for shock-compressed gold (120.3 GPa). The calculated results correspond to a compression of $V/V_0 = 0.752$ (120.3 GPa). The expected temperature is 2678 K (Fig. 4). The effect of varying this temperature by 1000 K is shown here. Green and blue dashed lines represent the calculated results at the same compression but at temperatures of 1678 and 3678 K, respectively. Also, the measured ambient x-ray diffraction line profile for gold is shown as the dotted blue curve.
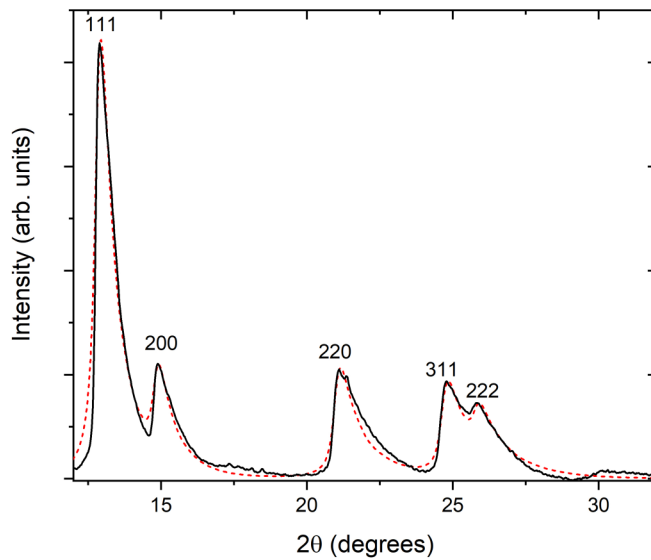

FIG. 8. Comparison of the experimental diffraction profile (solid black line) with the simulated profile (dashed red line) at ambient conditions for the five observed peaks of gold.
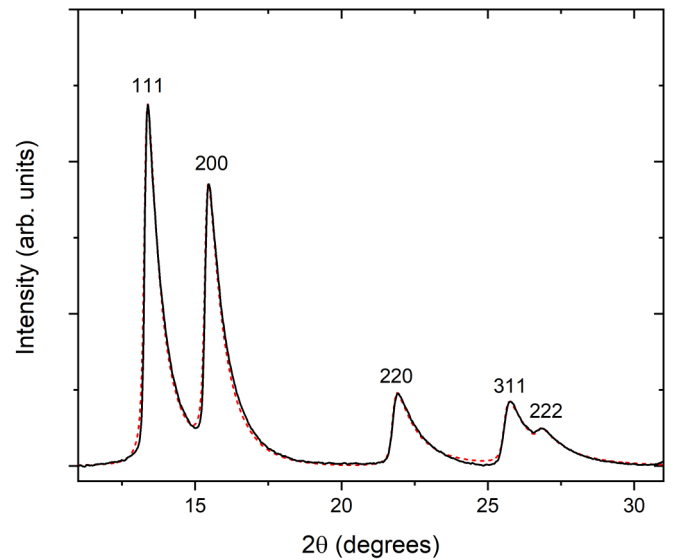

FIG. 10. Comparison of the experimental diffraction profile (solid black line) with the simulated profile (dashed red line) at ambient conditions for the five observed peaks of Pt.

[1] G. E. Duvall and R. A. Graham, Rev. Mod. Phys. **49**, 523 (1977).

[2] S. B. Kormer, M. V. Sinitsyn, G. A. Kirillov, and V. D. Urlin, Sov. Phys. JETP **21**, 689 (1965).

[3] G. A. Lyzenga, T. J. Ahrens, W. J. Nellis, and A. C. Mitchell, J. Chem. Phys. **76**, 6282 (1982).

[4] W. J. Nellis and C. S. Yoo, J. Geophys. Res. **95**, 21749 (1990).

[5] C. S. Yoo, N. C. Holmes, M. Ross, D. J. Webb, and C. Pike, Phys. Rev. Lett. **70**, 3931 (1993).

[6] D. Partouche-Sebban, D. B. Holtkamp, J. L. Pelissier, J. Taboury, and A. Rouyer, Shock Waves **11**, 385 (2002).

[7] T. M. Hartsfield, B. M. La Lone, G. D. Stevens, L. R. Veeser, and D. H. Dolan, J. Appl. Phys. **128**, 015903 (2020).

[8] B. J. Jensen, T. M. Hartsfield, D. B. Holtkamp, F. J. Cherne, R. B. Corrow, T. E. Graves, and A. J. Iverson, Phys. Rev. B **102**, 214105 (2020).

[9] Y. P. Opachich, R. S. Crum, M. W. Daene, E. C. Dutra, H. N. Mehta, H. L. Shelton, P. Watts, and M. C. Akin, Rev. Sci. Instrum. **91**, 033108 (2020).

[10] G. I. Pangilinan and Y. M. Gupta, Appl. Phys. Lett. **70**, 967 (1997).

[11] G. I. Pangilinan and Y. M. Gupta, J. Appl. Phys. **81**, 6662 (1997).

[12] A. Sato, S. Oguchi, and K. G. Nakamura, Chem. Phys. Lett. **445**, 28 (2007).

[13] D. Lacina and Y. M. Gupta, J. Chem. Phys. **141**, 084503 (2014).

[14] V. W. Yuan, J. D. Bowman, D. J. Funk, G. L. Morgan, R. L. Rabie, C. E. Ragan, J. P. Quintana, and H. L. Stacy, Phys. Rev. Lett. **94**, 125504 (2005).

[15] D. Kraus, A. Ravasio, M. Gauthier, D. O. Gericke, J. Vorberger, S. Frydrych, J. Helfrich, L. B. Fletcher, G. Schaumann, B. Nagler, B. Barbrel, B. Bachmann, E. J. Gamboa, S. Göde, E. Granados, G. Gregori, H. J. Lee, P. Neumayer, W. Schumaker, T. Döppner, R. W. Falcone, S. H. Glenzer, and M. Roth, Nat. Commun. **7**, 10970 (2016).

[16] S. J. Turneaure, N. Sinclair, and Y. M. Gupta, Phys. Rev. Lett. **117**, 045502 (2016).

[17] X. Wang, P. Rigg, J. Sethian, N. Sinclair, N. Weir, B. Williams, J. Zhang, J. Hawreliak, Y. Toyoda, Y. M. Gupta, Y. Li, D. Broege, J. Bromage, R. Earley, D. Guy, and J. Zuegel, Rev. Sci. Instrum. **90**, 053901 (2019).

[18] W. J. Murphy, A. Higginbotham, J. S. Wark, and N. Park, Phys. Rev. B **78**, 014109 (2008).

[19] R. P. Gupta and P. K. Sharma, J. Chem. Phys. **46**, 1359 (1967).

[20] N. Singh and P. K. Sharma, Phys. Rev. B **3**, 1141 (1971).

[21] C. K. Shepard, J. G. Mullen, and G. Schupp, Phys. Rev. B **61**, 8622 (2000).

[22] B. T. M. Willis and A. W. Pryor, *Thermal Vibrations in Crystallography* (Cambridge University Press, London, New York, 1975).

[23] B. E. Warren, *X-Ray Diffraction* (Addison-Wesley, Reading, MA, 1969).

[24] A. Matsumuro, M. Kobayashi, T. Kikegawa, and M. Senoo, J. Appl. Phys. **68**, 2719 (1990).

[25] K. Kusaba and T. Kikegawa, Solid State Commun. **149**, 371 (2009).

[26] S. M. Sharma, S. J. Turneaure, J. M. Winey, Y. Li, P. A. Rigg, A. Schuman, N. Sinclair, Y. Toyoda, X. Wang, N. Weir, J. Zhang, and Y. M. Gupta, Phys. Rev. Lett. **123**, 045702 (2019).

[27] S. M. Sharma, S. J. Turneaure, J. M. Winey, and Y. M. Gupta, Phys. Rev. Lett. **124**, 235701 (2020).

[28] S. M. Sharma, S. J. Turneaure, J. M. Winey, P. A. Rigg, N. Sinclair, X. Wang, Y. Toyoda, and Y. M. Gupta, Phys. Rev. X **10**, 011010 (2020).

[29] J. M. Walsh, M. H. Rice, R. G. McQueen, and F. L. Yarger, Phys. Rev. **108**, 196 (1957).

[30] C. W. Greeff and M. J. Graf, Phys. Rev. B **69**, 054107 (2004).

[31] G. E. Duvall and G. R. Fowles, in *High Pressure Physics and Chemistry*, edited by R. S. Bradley (Academic Press, New York, 1963), Vol. 2, pp. 209–291.

[32] M. Matsui, E. Ito, T. Katsura, D. Yamazaki, T. Yoshino, A. Yokoyama, and K. Funakoshi, J. Appl. Phys. **105**, 013505 (2009).

[33] T. Sun, K. Umemoto, Z. Wu, J. C. Zheng, and R. M. Wentzcovitch, Phys. Rev. B **78**, 024304 (2008).

[34] C. E. Wehrenberg, D. McGonegle, C. Bolme, A. Higginbotham, A. Lazicki, H. J. Lee, B. Nagler, H.-S. Park, B. A. Remington, R. E. Rudd, M. Sliwa, M. Suggit, D. Swift, F. Tavella, L. Zepeda-Ruiz, and J. S. Wark, Nature (London) **550**, 496 (2017).

[35] S. M. Sharma, S. J. Turneaure, J. M. Winey, and Y. M. Gupta, Phys. Rev. B **102**, 020103(R) (2020).

[36] S. J. Turneaure, P. Renganathan, J. M. Winey, and Y. M. Gupta, Phys. Rev. Lett. **120**, 265503 (2018).